Transition from the C$_3$-dominated discharge to the sooting plasma

Shoaib Ahmad,* Bashir Ahmad, and Tasneem Riffat

Accelerator Laboratory, PINSTECH, P. O. Nilore, Islamabad, Pakistan

(Received 8 February 2001; published 23 July 2001)

Mass spectrometry and photoemission spectroscopy of a graphite hollow cathode source identify the parameters of the transition from the C$_3$-dominated discharge to the sooting plasma. The transition is a function of the shape and profile of a special cusp magnetic field $B_z(r,\theta)$, the geometry of the source, the discharge current, and pressure. Characteristic atomic and molecular emission lines and bands in the C$_3$ discharge transform into broad bands emitted by the excited soot. We identify four prominent emission bands between 300–400 nm to be the hallmark of the sooting plasma.

I. INTRODUCTION

When a cylindrical graphite hollow cathode source is operated in the glow discharge mode with Ne or Ar, atomic and molecular carbon species (C$_1$,C$_2$,C$_3$, ...) are efficiently sputtered from the cathode. However, the initiation and sustenance of the discharge critically depend on the shape and intensity of the three-dimensional (3D) cusp magnetic field $B_z(r,\theta)$ generated by permanent magnets arranged in hexapole geometry and wrapped around the cylindrical source. Such a carbon cluster source is described in detail elsewhere [1]. By manipulating the geometry of the hollow cathode (HC), the hollow anode (HA) and the region of confinement of the cusp field $B_z(r,\theta)$, we reported the soot formation properties of this source [2]. The axial B_z, radial B_r and the azimuthal B_θ field contours produce the 3D magnetic field $B_z(r,\theta)$ that can be made to extend over the desired region of the plasma-cathode wall interactions. In this paper we provide evidence of the transition from a C$_3$-dominated discharge to the sooting plasma and highlight the parameters of this transition. Our experimental indicators are the mass spectrometry of the charged carbon clusters with a specially designed $E \times B$ velocity filter [3] and the photoemission spectroscopy of the source to determine the state of the carbon vapor. The source's geometrical and physical parameters allow us to achieve either a C$_3$-dominated discharge or a sooting plasma that may contain the entire range of the linear chains, rings and possibly, the closed caged carbon clusters—the fullerenes [2]. The most common feature of the carbon cluster formation from graphite by sputtering [1], laser ablation [4], and the high pressure arc discharge [5] involves the generation of the C bond breaking sequences from the graphite surface followed by the rebonding processes in carbon vapor. Investigations into the dynamics of the cluster formation in the hollow cathode source reveal that the cathode wall sputtering transforms the initial Ne$^+$-dominated discharge into a carbonaceous one. In such a multicomponent discharge all of its constituents recycle and regenerate the cathode deposited C clusters by kinetic ($E_{Ne^+,C_m}{}^+ \sim 500$–$1000$ eV) and potential ($E_{Ne^*,C_1}* \sim 10$–20 eV) sputtering. However, the potential sputtering by the

metastable Ne* is shown to be the most efficient regenerative agent for the clusters on the cathode surface [6].

Our present investigation into the role of the sputtering of the graphite hollow cathode by the plasma constituents yields useful information on certain similar aspects of the plasma wall sputtering in tokamak reactors. Whereas, we have designed the source to effectively enhance the wall erosion due to the plasma-wall interactions, the reverse is the requirement for the fusion reactors. Our conclusions are also valid for the studies of such processes in tokamaks. Our results show that the radial component of the extended 3D cusp magnetic field contours create an ideal environment for the entrapment of the charged particles. The subsequent interactions of the trapped, positively charged species with the cathode walls provide an efficient recycling mechanism for the wall deposited material. Therefore, we are purposefully relying on a particular source design that is to be avoided by the fusion reactor designers. In addition to providing an insight into the transition from a C$_3$-dominated discharge to the sooting plasma, we have presented the photoemissive signatures of a multicomponent carbon plasma and its regenerative behavior.

II. EXPERIMENT AND RESULTS

Schematic diagram of the source is shown in Fig. 1 with the discharge being generated and confined within the annular region between HC and HA. This is achieved by; (a) producing a threaded surface on the inside of HC so that a sharply peaked edge faces the anode, and (b) adjusting the cusp field $B_z(r,\theta)$ in the center of HA by specially designed soft iron rings described in Ref. [1]. Discharge species are extracted from the aperture in HC by a conical extractor (not shown in the figure). Three spectra are shown at different discharge currents i_{dis}. Figure 1(a) is at $i_{dis}=150$ mA, Fig. 1(b) at 37.5 mA and Fig. 1(c) is at 12.5 mA. All other experimental parameters remain the same. The peak labeled C$_3^+$ is the main feature while the Ne$^+$ shifts to lower energy in Fig. 1(b) and disappears in Fig. 1(c). In the insets are the enlarged peaks of C$_1^+$ and C$_2^+$ with their respective magnification factors. The other variable intensity features, besides the sharply peaked Ne$^+$, are broad humps labeled as C$_3^{2+}$ and C$_3^{4+}$. The respective spectra in Figs. 1(a)–1(c) are obtained at gradually decreasing i_{dis}. Therefore, the most con-

---

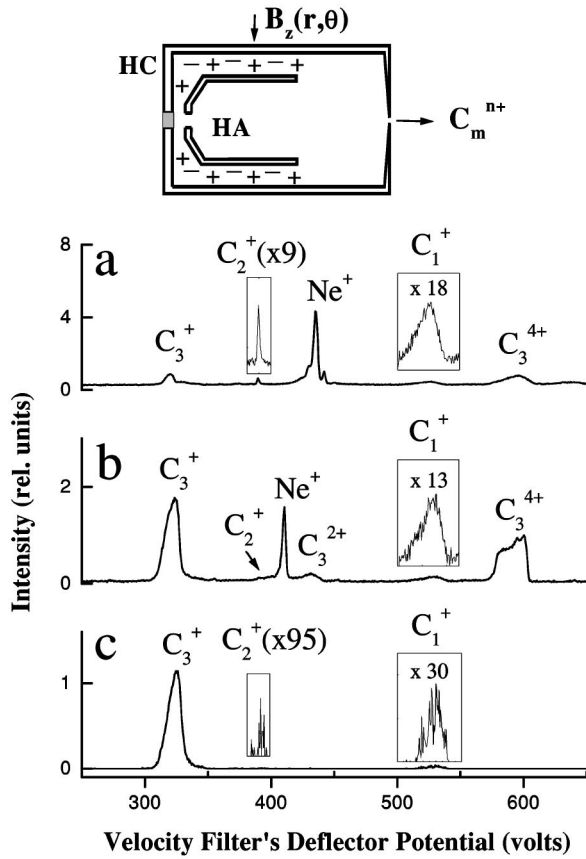*Corresponding author: Email address: shoaib@pinstech.org.pk

FIG. 1. The schematic diagram of the source is shown with the discharge being generated between the HC and HA. The cusp magnetic field $B_z(r, \theta)$ is confined in the center of HA. Charged carbon clusters C_m^{n+} ($m, n \geqslant 1$) are extracted by a conical extractor (not shown in the figure). (a) $i_{dis} = 150$ mA, Ne$^+$ is the most significant peak followed by C_3^+ and C_3^{4+}. Inset: C_2^+ and C_1^+ are shown magnified by a factor of 9 and 18, respectively. (b) $i_{dis} = 37.5$ mA, C_3^+ is the most prominent mass peak with Ne$^+$, C_3^{2+}, and C_3^{4+}. C_2^+ is only indicated by an arrow. Inset: C_1^+ is 13 times enlarged. (c) $i_{dis} = 12.5$ mA, C_3^+ is the only and most significant peak. Inset: C_2^+ and C_1^+ are shown by their respective enlargement factors.
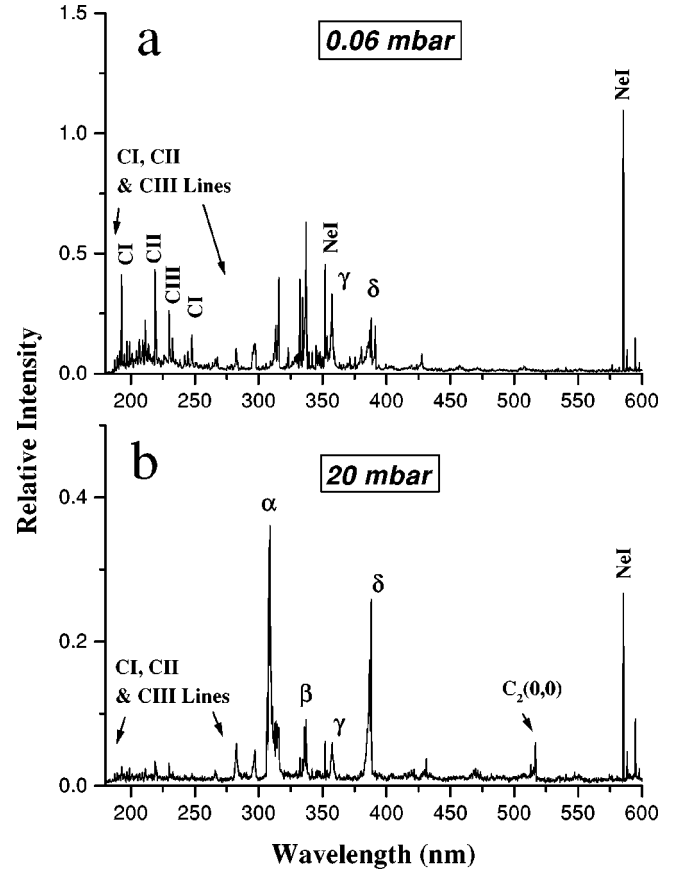
FIG. 2. (a) Photoemission spectrum at $i_{dis} = 75$ mA, $P_{Ne} = 0.06$ mbar. The atomic and ionic lines are sharply defined and indicated as C I, Ne I, C II, and C III. Also shown are the two band structures at 357 nm and 385 nm are designated as γ and δ, respectively. (b) Photoemission spectrum at $i_{dis} = 75$ mA and $P_{Ne} = 20$ mbar shows the greatly reduced intensities of the atomic and ionic lines of C and Ne. The four bands labeled as α, β, γ, and δ are the prominent feature of this emission spectrum. The Swan band head of C_2 [$C_2(0,0)$] at $\lambda = 5165$ Å is also present with enhanced intensity.

vincing proof of the discharge being dominated by C_3^+ comes from Fig. 1(c) that is obtained at $i_{dis} = 12.5$ mA ($P_{dis} = 8$ W). We cannot ignite the source at such low power but once a stable discharge is established, the source can operate at substantially reduced i_{dis}. But this can only happen if one has a multicomponent plasma and at least one of the species has high metastable energy levels; in this case it is Ne* ($E_{Ne*} \approx 16.7$ eV). The pattern of sputtering and formation of the excited and ionized $C_1^{*,+}$ and C_2^* from this source has been reported as a function of the discharge parameters [6]. These species become the agents for the formation of the C cluster layers on the cathode. Our experimental results suggest that the subsequent recycling and regeneration of these layers result in the formation of the C_3^+ dominated discharge as is shown in Fig. 1(c).

The role of the kinetic and potential sputtering has been evaluated in the regeneration of the soot [6]. One can either

vary the i_{dis} at constant gas pressures to manipulate the number of ionized and excited species or vary the support gas pressure P_{Ne} while keeping i_{dis} constant. This provides a powerful tool to investigate the mechanisms of cluster formation and dissociation in a carbonaceous environment. However, the mass spectrometry of the charged clusters at very high pressures becomes difficult due to vacuum problems. We use photoemission spectroscopy of the discharge at such high pressures and relate the information available from the characteristic lines and band emission from the excited atomic, ionic, and molecular species to that obtained by the mass analysis. Figure 2 shows two such spectra at different source pressures but with the same $i_{dis} = 75$ mA. Pressure is increased by more than two orders of magnitude from $P_{Ne} = 0.06$ mbar in Fig. 2(a) to 20 mbar in Fig. 2(b). The relative line intensities of the emission lines of C, Ne, and four bands identified as α, β, γ, and δ are shown between 180–600 nm. Atomic lines are sharp while the individual lines of the bands cannot be separated by our monochromator. Most
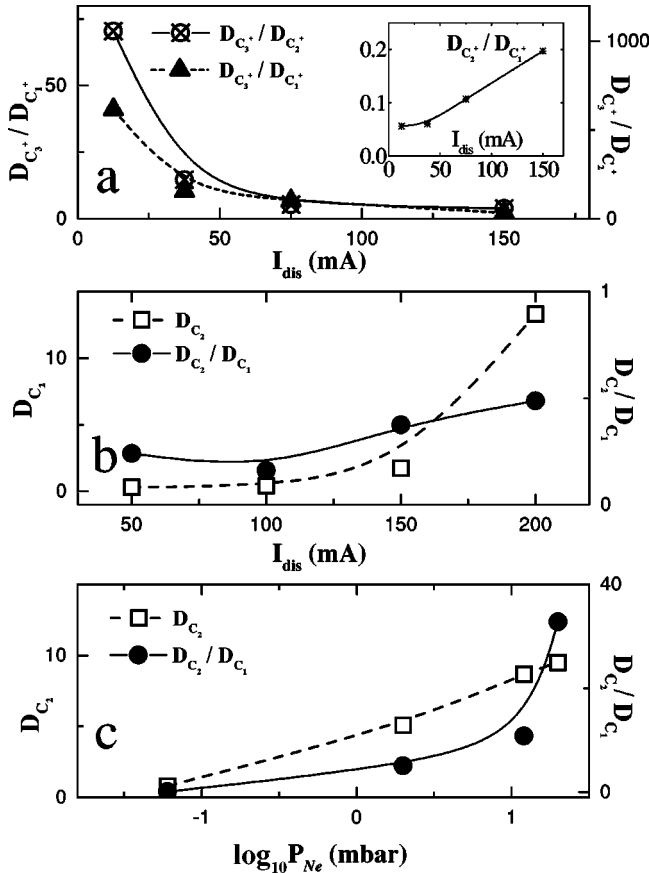
FIG. 3. (a) The ratios of the ion densities $D_{C_3^+}/D_{C_1^+}$ and $D_{C_3^+}/D_{C_2^+}$ are plotted as a function of i_{dis}. C_3^+ is the main plasma constituent and its contribution increases at lower i_{dis}. Inset: The ratio $D_{C_2^+}/D_{C_1^+}$ is shown for the same range of i_{dis}. (b) At $P_{Ne}=0.06$ mbar the photoemission spectra yield the number densities of the lowest vibrationally excited transition of C_2's Swan band $[C_2(0,0)]$ at $\lambda=5165$ Å and its ratio with the excited atomic C atoms (C I) at $\lambda=2478$ Å denoted as D_{C2}/D_{C1} is plotted as a function of i_{dis}. Same as FIG. 3(b) but with $i_{dis}=75$ mA and the discharge variable being P_{Ne} between 0.06 and 20 mbar. The D_{C_2}/D_{C_1} ratio rises steeply after $P_{Ne}>1$ mbar.

conspicuous is the resonant line of Ne I at $\lambda=5852$ Å in Fig. 2(a) and 2(b). A set of lines belonging to the excited atomic C_1^* i.e., C I at $\lambda=1931$ Å and 2478 Å, the intercombination multiplet of the singly charged C_1^+ i.e., C II at $\lambda=2324-2328$ Å and the doubly charged C_1^{++} i.e., C III at $\lambda=2297$ Å are shown in the range 180–300 nm. Between 300 and 400 nm, we get a large number of prominent lines and bands, the origin of which we will discuss here and also in a later section while dealing with the photoemission spectra of the sooted plasmas. The vibrationally excited Swan band head of $C_2(0,0)$ at $\lambda=5165$ Å is the other most important feature at higher pressures. It is present at low pressures as well but acquires significant proportions as the pressure is increased.

The accumulated data for the relative ion densities of C_3^+ $(D_{C_3^+})$, C_2^+ $(D_{C_2^+})$, and C_1^+ $(D_{C_1^+})$ as functions of i_{dis} and P_{Ne} are presented in Fig. 3. In Fig. 3(a) the ratios

of $D_{C_3^+}/D_{C_1^+}$ and $D_{C_3^+}/D_{C_2^+}$ are plotted as a function of i_{dis} from 12.5 to 150 mA. C_3^+ is the sole survivor at very low discharge currents. Its relative number density increases with respect to that of C_1^+ by a factor of 27 between $i_{dis}=150$ and 12.5 mA. Whereas, $D_{C_3^+}/D_{C_2^+}$ increases by two orders of magnitude as i_{dis} is decreased in the same range. This pattern is clearly evident from Fig. 1(c). In the inset of Fig. 3(a) $D_{C_2^+}/D_{C_1^+}$ is shown for the same range of i_{dis}. The number density of C_2^+ ($D_{C_2^+}$) increases from 5% to 20% of C_1^+ ($D_{C_1^+}$). Figures 3(b) and 3(c) show the number densities of the excited states of C_2 and C_1 as functions of i_{dis} and P_{Ne}, respectively. We have derived the number densities of the excited C_1^* and C_2^* from the line intensities of the electronically excited C I at $\lambda=2478$ Å and the lowest transition of the Swan band with the vibrationally excited $C_2(0,0)$ at $\lambda=5165$ Å. The number densities of $C_2(0,0)$ denoted as D_{C_2} are plotted on the left vertical axis and the ratio D_{C_2}/D_{C_1} along the right vertical axis for i_{dis} between 50 and 200 mA. It can immediately be seen that the density of $C_2(0,0)$ is an increasing function of both of the discharge parameters i_{dis} and P_{Ne}. The number density of the excited state of neutral C_1 i.e., C I also increases rapidly with i_{dis}, but its contribution is reduced at higher pressures as can be seen in Fig. 2(b). That is why the D_{C_2}/D_{C_1} ratio in Fig. 3(b) does not vary as steeply as it does in Fig. 3(c). From the photoemission data the ratio of the singly charged to the excited C i.e., $D_{C\,II}/D_{C\,I}$ remain constant, for example in the range of $P_{Ne}=0.1-1$ mbar it is 0.55 ± 0.2 for $i_{dis}=50-200$ mA. Similarly $D_{C_2(0,0)}/D_{CI}=2.2\pm0.4$ under the same conditions. At low pressure discharge i.e., $P_{Ne}\leq1$ mbar the charged atomic carbon C_1^+ (C II) and the excited diatomic molecular carbon $[C_2(0,0)]$ are directly related with C I i.e., C_1 in the $^1P_1$ level ($E_{1P_1}\approx7.5$ eV). Thus it may be deduced that the origin of C_1 and C_2 is in the dissociation of C_3 via $C_3\rightarrow C_2+C_1$. From the tabulated data presented in Fig. 3 we conclude that C_3^+ is not only the significant species at low i_{dis} but is the main constituent of the discharge under the experimental conditions as elucidated in Fig. 1. It may be due to the regeneration pattern of all clusters C_m^+ $(m>3)$ up to C_{30} that favors the accumulation of C_3 as the end product [7–9]. This fragmentation scheme $C_m^+ \xrightarrow{(5.5\pm0.5\ \text{eV})} C_{m-3}^+ + C_3$ has been predicted in the *ab initio* calculations [7] of C_m^+ up to $m=10$ and the experiments for all C_m^+ up to $m\leq60$ [8,9]. C_3 can itself dissociate into C_2 and C_1 ($C_3 \xrightarrow{(7\pm0.5\ \text{eV})} C_2+C_1$) and $C_2\rightarrow2C_1$. This fragmentation pattern can explain not only the preponderance of C_3 but also the enhanced contribution of C_1 at higher i_{dis}. But at higher P_{Ne}, the large relative increase in the density of C_2 cannot be explained by the C_3 fragmentation. At $P_{Ne}>1$ mbar, the increased contribution from the $C_2(0,0)$ is accompanied by the corresponding increase in the bands emission in 300–400 nm and a consequent decrease in the excited and ionic states of the atomic carbon C_1 (C I, C II, C III) lines as seen in Fig. 2(b). We interpret it
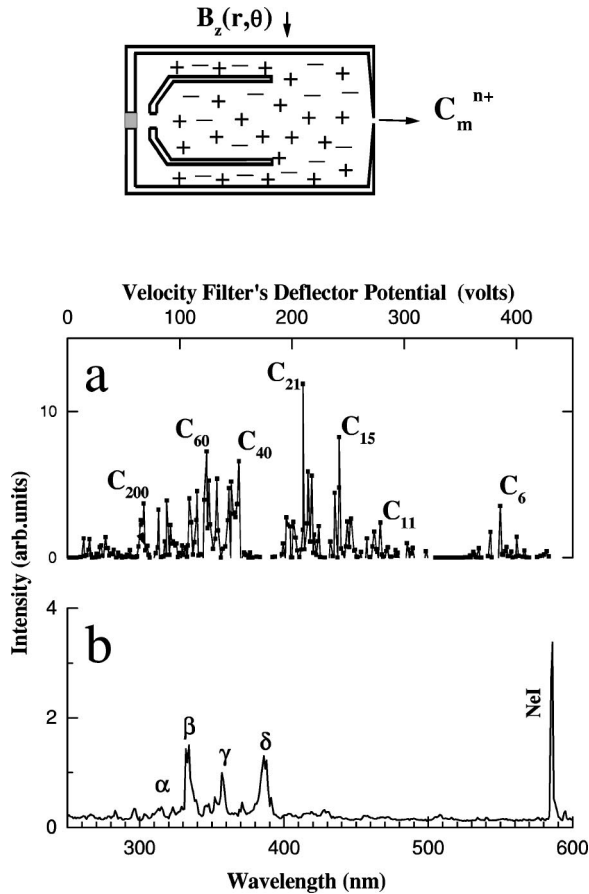
FIG. 4. The source is shown in the sooting mode with the cusp magnetic field $B_z(r,\theta)$ providing discharge conditions in the main HC. (a) A typical mass spectrum of the clusters C_m^{n+} is shown. Beyond C_6^{+}, no significant ions are seen. (b) The photoemission spectrum from the sooted source operating with the same discharge parameters as in (a). Besides the ubiquitous Ne I $\lambda = 5852$ Å line, the significant emissions are from the bands α, β, γ, and δ at 310, 337, 357, and 385 nm, respectively.

as the onset of the formation of the closed caged clusters C_m ($m > 30$). These clusters further fragment via C_2 emission $C_m(m \geqslant 30) \rightarrow C_{m-2} + C_2$ [4]. This is our preferred interpretation of the enhanced $C_2(0,0)$ intensities at $P_{Ne} > 10$ mbar.

The schematic diagram in Fig. 4 shows the hollow cathode source operating in the sooting mode. The magnetic cusp field provides conditions of discharge in the main HC region and is no longer confined to the annular region between HA and HC as was done to operate the source in the C_3-dominated mode shown in Fig. 1. A typical cluster spectrum is shown from this source configuration in Fig. 4(a) that is taken from Ref. [2]. It shows clusters labeled from C_1 to C_{200}, however, larger clusters are also present in the spectrum. The sooting mode shown here may be related to the regenerative processes initiated by the plasma-sooted cath-

ode interactions. As pointed out in the C_3-dominated discharge, the regeneration of the soot layers takes place mostly by the excited and metastable plasma species like Ne* and C_1^* with $E_{Ne*} \approx 16.7$ eV and $E_{C_1^*} \approx 7.5$ eV, respectively. Figure 4(b) shows the photoemission spectra taken with the four broad and prominent bands designated as $\alpha, \beta, \gamma, \delta$ appearing at almost the same wavelengths as in Fig. 2(b). The band heads of α, β, γ, and δ are at 310, 337, 357, and 385 nm, respectively. Out of these four bands, α degrades to the red, δ to the violet while β and γ are symmetrically disposed. Referring to Figs. 2(a) and 2(b), γ and δ seem to be the band emissions from C_2 and C_3. Therefore, α and β may be associated with the closed caged clusters shown in Fig. 4(a).

III. CONCLUSION

In conclusion we have presented in this paper, the parameters for the initiation of a C_3-dominated discharge in a graphite hollow cathode that operates in a special cusp magnetic field configuration. We have shown that the transition from the C_3 to the sooted plasma is dependent upon the source geometry, the field configuration, and the discharge parameters. Mass spectra provide clear evidence of the dominant plasma species while operating either in the C_3-dominated regime or the sooting mode. The photoemission spectroscopy yields the characteristic emissive pattern in the form of four UV bands in the range 300–400 nm associated with the dominant carbon cluster species. Our tentative interpretation of these bands in the light of the emission spectra shown in Ref. [6] and our present mass spectra shown in Figs. 1 and 4(a), respectively, is that γ and δ may be due to the excited vibrational states of C_2 and C_3 as both species may be produced in the initial sputtering processes as well as during the subsequent fragmentation as discussed in the previous section. On the other hand, the bands designated as α and β seem to be associated with the onset of the formation of the closed caged clusters, i.e., the fullerenes and perhaps the multishelled carbon onions [2].

We have discussed the formation of the soot by the overall process of recycling and introduction of the cathode deposited carbon clusters. Once the $C_3 \rightarrow$ soot transition has been made, an entire range of clusters is produced in the regenerative sooting plasma. We are planning to use this graphite hollow cathode source for establishing the upper limit on the largest, free standing, monoshelled fullerenes that can be extracted from the regenerative soot. The other equally interesting question is regarding the onset of the formation of the multishelled carbon onions. In addition, this sooting plasma source can inject a particular carbon clusters $C_m^+(m > 2)$ into the beam line of any accelerator for various basic and applied studies with the carbon clusters. As we have also indicated the essential features of a soot forming discharge in magnetized plasmas contained within the graphite cathodes, this information may be of interest to the fusion reactor designers.

[1] S. Ahmad and T. Riffat, Nucl. Instrum. Methods Phys. Res. B **152**, 506 (1999).

[2] S. Ahmad, Phys. Lett. A **261**, 327 (1999); Eur. Phys. J.: Appl. Phys. **5**, 111 (1999).

[3] S. Ahmad, B. Ahmad, A. Qayyum, and M. N. Akhtar, Nucl. Instrum. Methods Phys. Res. A **452**, 371 (2000).

[4] H. W. Kroto, J. R. Heath, S. C. O'Brien, R. F. Curl, and R. E. Smalley, Nature (London) **318**, 162 (1985).

[5] W. Krätschmer, L. D. Lamb, K. Fostiropoulous, and D. R. Huffman, Nature (London) **347**, 354 (1990).

[6] S. Ahmad, A. Qayyum, M. N. Akhtar, and T. Riffat, Nucl. Instrum. Methods Phys. Res. B **171**, 552 (2000); S. Ahmad and M. N. Akhtar, Appl. Phys. Lett. **78**, 1499 (2001).

[7] K. Raghavachari and J. S. Binsky, in *Physics and Chemistry of Small Clusters*, Vol. 150 of *NATO Advanced Studies Institute, Series B: Physics*, edited by P. Jena *et al.* (Plenum Press, New York, 1987), p. 317; J. Chem. Phys. **87**, 2191 (1987).

[8] S. W. McElvany, B. I. Dunlop, and A. O'Keefe, J. Chem. Phys. **86**, 715 (1987).

[9] P. P. Radi, T. L. Bunn, P. R. Kemper, M. E. Molchn, and M. T. Bowers, J. Chem. Phys. **88**, 2809 (1988).